Schmidt number effects on turbulent transport with uniform mean scalar gradient

P. K. Yeung[a] and Shuyi Xu
School of Aerospace Engineering, Georgia Institute of Technology, Atlanta, Georgia 30332

K. R. Sreenivasan[b]
Institute for Physical Science and Technology, University of Maryland, College Park, Maryland 20742

(Received 18 April 2002; accepted 6 September 2002; published 18 October 2002)

We study by direct numerical simulations the effects of Schmidt number (Sc) on passive scalars mixed by forced isotropic and homogeneous turbulence. The scalar field is maintained statistically stationary by a uniform mean gradient. We consider the scaling of spectra, structure functions, local isotropy and intermittency. For moderately diffusive scalars with $Sc=1/8$ and 1, the Taylor-scale Reynolds number of the flow is either 140 or 240. A modest inertial-convective range is obtained in the spectrum, with a one-dimensional Obukhov–Corrsin constant of about 0.4, consistent with experimental data. However, the presence of a spectral bump makes a firm assessment somewhat difficult. The viscous-diffusive range is universal when scaled by Obukhov–Corrsin variables. In a second set of simulations we keep the Taylor-microscale Reynolds number fixed at 38 but vary Sc from 1/4 to 64 (a range of over two decades), roughly by factors of 2. We observe a gradual evolution of a -1 roll-off in the viscous-convective region as Sc increases, consistent with Batchelor's predictions. In the viscous-diffusive range the spectra follow Kraichnan's form well, with a coefficient that depends weakly on Sc. The breakdown of local isotropy manifests itself through differences between structure functions with separation distances in directions parallel and perpendicular to the mean scalar gradient, as well as via finite values of odd-order moments of scalar gradient fluctuations and of mixed velocity-scalar gradient correlations. However, all these indicators show, to varying degrees, an increasing tendency to isotropy with increasing Sc. The moments of scalar gradients and the scalar dissipation rate peak at $Sc\approx 4$. The intermittency exponent for the scale-range between the Kolmogorov and Batchelor scales is found to decrease with Sc, suggesting qualitative consistency with previous dye experiments in water $[Sc=O(1000)]$. [DOI: 10.1063/1.1517298]

I. INTRODUCTION

The properties of small-scale turbulence are of interest for a number of reasons (see, e.g., Refs. 1–3). For passive scalars, the small-scale structure is influenced, besides the Reynolds number, by the Schmidt number, $Sc\equiv \upsilon/D$, where υ is the kinematic viscosity of the fluid and D is the molecular diffusivity of the scalar. Because Sc can vary widely in applications (from order 10^{-3} in liquid metals to order unity in gaseous flames to thousands and higher in organic mixtures and biological fluids), an understanding of its influence is important. This understanding is currently limited. This paper attempts to remedy the situation to some degree, with emphasis on Sc of order unity and higher. The background turbulence is stationary, homogeneous, and isotropic, and the scalar is maintained by a uniform mean gradient. We use direct numerical simulations (DNS) and consider spectra, structure functions, local isotropy and intermittency.

Regarding spectra, a well-known result for $Sc\approx 1$ is that based on classical extensions of Kolmogorov's arguments[4] by Obukhov[5] and Corrsin:[6] A $k^{-5/3}$ roll-off rate (where k is the wavenumber) in the so-called inertial-convective range at sufficiently high Reynolds numbers, and a viscous-diffusive range that is similar to the dissipative region for the velocity but parameterized by Sc (see Ref. 1). For scalars with $Sc \gg 1$, the spectral forms proposed by both Batchelor[7] and Kraichnan[8] include an in-between k^{-1} range. In experiments, the $-5/3$ region (with possible intermittency corrections) has been observed quite often; for recent summaries, see Sreenivasan[9] and Mydlarski and Warhaft.[10] On the other hand, available evidence on the k^{-1} range is mixed: Gibson and Schwarz[11] and Prasad and Sreenivasan[12] favor its existence but Miller and Dimotakis[13] and Williams *et al.*[14] do not. Numerical experiments by Holzer and Siggia,[15] although based on two-dimensional synthetic velocity fields, do appear to support Batchelor scaling of the scalar spectrum.

Structure functions of different orders have been studied by a number of investigators (see, for example, Antonia *et al.*,[16] Meneveau *et al.*,[17] Moisy *et al.*,[18] Skrbek *et al.*,[19] each of which emphasizes different aspects related to this

[a]Telephone: 1-404-894-9341; fax: 1-404-894-2760. Electronic mail: yeung@peach.ae.gatech.edu
[b]Telephone: 1-301-405-4878; fax: 1-301-314-9363. Electronic mail: sreeni@ipst.umd.edu

TABLE I. Major parameters of the numerical simulations.

N	64	64	256	256	256	512	512	512	256	256	512	512
R_λ	38	38	38	38	38	38	38	38	140	140	240	240
Sc	1/4	1	4	8	16	16	32	64	1/8	1	1/8	1
$k_{\max}\,\eta$	1.44	1.44	5.94	5.94	5.94	11.81	11.81	11.81	1.42	1.42	1.39	1.39
$k_{\max}\,\eta_B$	2.88	1.44	2.97	2.10	1.48	2.95	2.09	1.48	4.00	1.42	3.93	1.39
$\rho_{u\phi}$	−0.64	−0.56	−0.48	−0.45	−0.42	−0.45	−0.42	−0.40	−0.59	−0.53	−0.59	−0.56
r_ϕ	2.65	1.78	1.26	1.09	0.95	0.98	0.87	0.77	3.06	2.36	2.71	2.33
$\langle\phi^2\rangle$	1.29	2.13	3.11	3.61	4.13	3.99	4.51	5.04	1.71	2.26	3.17	3.68
$\langle\chi\rangle$	2.46	2.74	2.76	2.77	2.76	2.71	2.70	2.70	1.97	2.00	3.22	3.22

same issue), but there is a lack of data on Schmidt number dependence. In particular, the velocity-scalar mixed structure function of third-order, for which an exact asymptotic result at intermediate scales is known from Yaglom,[20] has not been studied in detail.

The concept of local isotropy for small-scale turbulence is well known. Recent reviews (e.g., Sreenivasan,[21] Warhaft[22]) have emphasized that passive scalars show first-order deviations from it when a mean gradient is present. However, most of the data that form the basis of the conclusion are for $Sc=O(1)$. It is reasonable to speculate that, when $Sc\gg 1$, the separation between the Kolmogorov scale (η) and the Batchelor scale ($\eta_B, \equiv \eta Sc^{-1/2}$) plays an important role, and that the scalar fluctuations may be more nearly isotropic at higher Sc.

An important property of high-Reynolds-number turbulence is intermittency, in the form of short-lived or localized bursts of intense fluctuations often associated with the small scales. Numerous studies based on both experimental and numerical work (e.g., Refs. 3, 21–24) have shown that the passive scalar is more intermittent than the velocity. An important issue is the nature of this behavior for $Sc\gg 1$. Some experimental data (e.g., Sreenivasan and Prasad[25]) have suggested a lack of intermittency in the Batchelor range between η and η_B.

The challenge in studying these problems for $Sc\gg 1$ is the need to resolve scalar fluctuations at the smallest scales. In order to compute them without losing accuracy, progressively finer grids must be employed and the Reynolds number has to be held at moderately low values. This may seem discouraging. However, Batchelor scaling relies essentially on the scale separation between η and η_B and does not involve the large scales. Limitations on the Reynolds number are thus less crucial. While DNS has been used in the past to study mixing for $Sc>1$, with the exception of some new data at $Sc=144$ by Brethouwer *et al.*,[26] it is mostly limited[27,28] to $Sc<10$. Further, these previous studies have not provided the data that we shall report here.

We use data from a series of direct numerical simulations with a uniform mean scalar gradient, with the Schmidt number varied systematically from 1/4 to 64. This range is thought to be wide enough to detect trends with Sc. The simulation conditions are summarized in Sec. II. Results on the scalar spectrum and structure functions are presented in Sec. III. In Sec. IV we examine the issue of local isotropy, mainly in terms of derivative statistics in directions parallel or perpendicular to the mean scalar gradient. In Sec. V we consider the characterization of intermittency. Conclusions are summarized in Sec. VI.

II. NUMERICAL SIMULATION PARAMETERS

Our numerical simulations were performed using a version of the Fourier pseudo-spectral algorithm of Rogallo,[29] which has been adapted for use on massively parallel computers. We focus on the behavior of passive scalar fluctuations, ϕ, evolving in forced isotropic turbulence in the presence of a uniform mean scalar gradient, $\nabla\Phi$. The governing equation is

$$\frac{\partial\phi}{\partial t}+u_i\frac{\partial\phi}{\partial x_i}=-u_i\frac{\partial\Phi}{\partial x_i}+D\frac{\partial^2\phi}{\partial x_i\partial x_i}. \tag{1}$$

The presence of the mean gradient, which is taken to be $\nabla\Phi=(G,0,0)$ in a Cartesian coordinate system, means that at least some of the statistics of the scalar field may be anisotropic. The velocity and scalar fields are statistically stationary in time, although substantial temporal variations of space-averaged statistics such as turbulence kinetic energy, K, can occur (e.g., Overholt and Pope[23]). Stationarity allows data taken at different times to be used as multiple realizations for the purpose of ensemble averaging. Data sets for post-processing analysis are usually saved at intervals on the order of one eddy-turnover time (T_e, the ratio of longitudinal integral length scale to r.m.s. velocity).

Several major simulation parameters are summarized in Table I. The simulations are in two groups. In the first of these, the Schmidt number is varied from 1/4 to 64 while the Taylor-scale Reynolds number (R_λ) is kept constant at 38. The resolution criterion applicable for $Sc>1$ is that the parameter $k_{\max}\,\eta_B$ (where $k_{\max}=\sqrt{2}N/3$ is the highest wavenumber resolved on an N^3 grid) should be at least 1.5. This criterion is met by a 256^3 run with three scalars at $Sc=4$, 8, 16, and a 512^3 run with $Sc=16$, 32, 64. Comparisons between $Sc=16$ data simulated on 256^3 and 512^3 grids serve as a check on the effects of finite numerical resolution. In the second set of simulations we address Reynolds number effects for $Sc\leqslant 1$. The highest two Reynolds numbers ($R_\lambda\approx 140$ and 240) are sufficient to yield a well-defined, though limited, inertial range in the energy spectrum (Yeung and Zhou[30]). To help ensure adequate sampling we have taken data from DNS spanning a time period on the order 10 eddy-turnover times.

In Table I it can be seen that, for fixed velocity parameters, as Sc increases the variance $\langle\phi^2\rangle$ of the scalar in-

creases steadily, while its dissipation rate, $\langle\chi\rangle$, remains nearly constant. (The behavior of $\langle\chi\rangle$ is discussed in detail in a separate paper.[31]) When the scalar field is statistically stationary, balance between the production of scalar variance due to the mean gradient and dissipation by molecular action requires that

$$-\rho_{u\phi}u'\phi'G=\langle\chi\rangle, \tag{2}$$

where the primes denote root-mean-square fluctuations, and $\rho_{u\phi}$ is the velocity-scalar correlation coefficient. The value of $\rho_{u\phi}$ is of order -0.5 for $Sc=O(1)$, and its magnitude decreases as Sc increases. Table I also gives the ratio of the mechanical time scale to the scalar time scale, $r_\phi=(K/\langle\epsilon\rangle)/(\langle\phi^2\rangle/\langle\chi\rangle)$, where $\langle\epsilon\rangle$ is the energy dissipation rate. The ratio r_ϕ is an important parameter in many studies of turbulent mixing (e.g., Warhaft and Lumley,[32] Eswaran and Pope[33]). In simplified mixing models r_ϕ is often (see Pope[34]) set to be 2.0. However, as reported separately elsewhere,[35] Table I shows that r_ϕ decreases with both Reynolds number and Schmidt number, becoming systematically below 1.0 for higher Sc; thus, in general (e.g., Fox[36]), the Schmidt number dependence of r_ϕ must be incorporated in modeling.

The Schmidt number dependence seen in Table I is in contrast to the observation in studies of differential diffusion of scalars of different molecular diffusivities (e.g., Yeung and Pope[37]) where the large scales are found to be almost independent of Schmidt number. However, at a finite Reynolds number the small scales do have non-negligible contributions to quantities like $\rho_{u\phi}$ and r_ϕ. In particular, as Schmidt number increases, the scalar variance increases slightly since weaker diffusivity allows scalar fluctuations to become locally more intense; yet scalar dissipation is almost constant. This effect softens at higher Reynolds number, when the large scales make more dominant contributions to scalar variance, and when blobs of high scalar concentration are more readily broken up by the effects of turbulent advection.

III. SPECTRUM AND STRUCTURE FUNCTIONS

A. Moderately diffusive scalars

For scalars with $Sc\leqslant 1$, effects of molecular diffusion are dominant for scales smaller than the Obukhov–Corrsin (OC) scale, $\eta_{\rm OC}=\eta Sc^{-3/4}$. The usual high-Reynolds-number arguments yield an inertial-convective range of wavenumbers $1/L\ll k\ll 1/\eta_{\rm OC}\leqslant 1/\eta$ (where L is an integral length scale of the flow) in which the spectrum has the form

$$E_\phi(k)=C_\phi^*\langle\chi\rangle\langle\epsilon\rangle^{-1/3}k^{-5/3}. \tag{3}$$

Here C_ϕ^* is the Obukhov–Corrsin constant. To compare our data with Eq. (3), we plot in Fig. 1 the ''compensated'' three-dimensional spectrum corresponding to the suggested scaling, for scalars with $Sc=1/8$ and 1, at three different Reynolds numbers. At higher R_λ a narrow flat region is seen to develop, extending towards the lower wavenumbers (for $R_\lambda\approx 240$, centered around $k\eta\approx 0.03$). For $Sc=1$ we also observe a spectral ''bump'' which is most pronounced at around $k\eta\approx 0.2$, independent of the Reynolds number. Reynolds number similarity for high wavenumbers is also reflected by

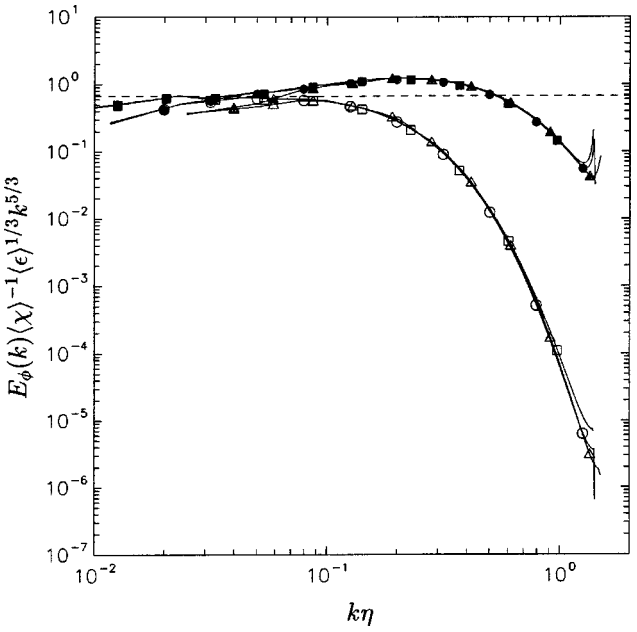

FIG. 1. Compensated spectrum according to Obukhov–Corrsin variables [Eq. (3)] for passive scalars at different Schmidt numbers (open symbols for 1/8, closed symbols for 1.0). Triangles, circles and squares denote ensemble-averaged Taylor-scale Reynolds numbers of 90, 140, and 240, respectively. Dashed line at 0.67 is for comparison with experiments.

the ''collapse'' at high wavenumbers for different R_λ but fixed Sc. On the other hand, a similar collapse occurs at low wavenumbers for different Sc but fixed R_λ. The latter feature is consistent with other results showing that the effects of differential diffusion are primarily found in small scales.[37–39]

Although it is straightforward to compute in DNS the spectrum in Eq. (3) as a function of wavenumber magnitude in three-dimensional space, experiments usually measure only the one-dimensional version $E_{1\phi}(k)$. In particular, if isotropy were valid, we have[1]

$$E_\phi(k)=-k\frac{dE_{1\phi}(k)}{dk}. \tag{4}$$

This relation implies that the Obukhov–Corrsin constant C_ϕ^* in the three-dimensional spectrum should be 5/3 of C_ϕ, the latter being the one-dimensional constant. It follows that the experimental value[9] of $C_\phi\approx 0.4$ corresponds to $C_\phi^*=0.4(5/3)=0.67$. A test of isotropy for the spectra can be made by taking the ratio of both sides in Eq. (4); this ratio is very close to unity except in the two lowest wavenumber shells, which correspond to the largest scales for which only a limited number of samples exist in the computational domain.

Figure 2 shows the one-dimensional compensated spectrum, for scalars with $Sc=1/8$ and 1 at $R_\lambda\approx 240$. We have taken an average over three coordinate directions. To infer C_ϕ accurately we have used a linear scale for the ordinate and included a dashed line corresponding to the experimental value in Ref. 9. Although the range is narrow, there is some evidence for scaling with the right value of the Obukhov–Corrsin constant. The spectral bump (for $Sc=1$) is quite conspicuous. The bump occurs within about the same range

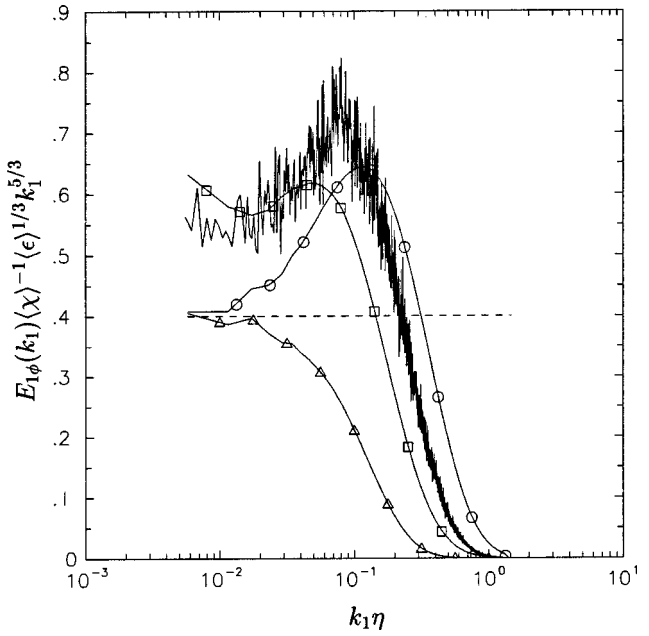

FIG. 2. Compensated one-dimensional spectrum for scalars of $Sc=1/8$ (triangles) and $Sc=1$ (circles) at $R_\lambda \approx 240$. Dashed line at 0.4 is for comparison with experiments (see Ref. 9). Also shown for comparison are: Squares for one-dimensional longitudinal energy spectrum in DNS, and unmarked solid line for data on scalar spectrum from Ref. 10 at R_λ 582 and Prandtl–Schmidt number 0.71.

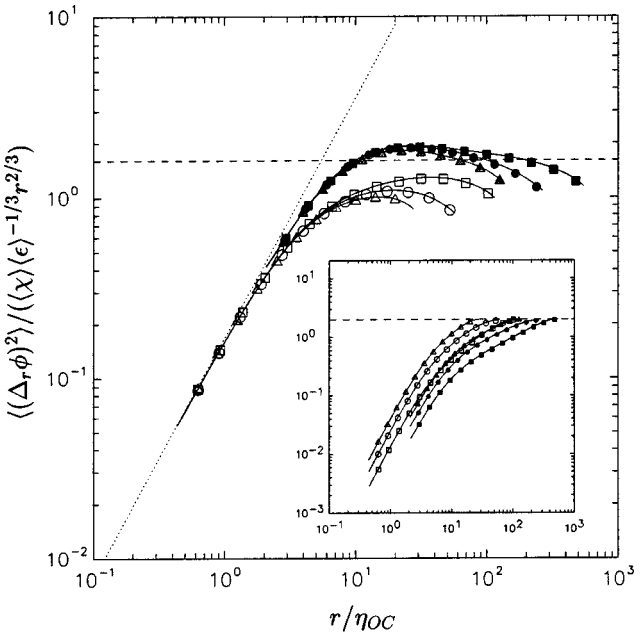

FIG. 3. Obukhov–Corrsin scaling of component-averaged second-order structure function of passive scalars at different Schmidt numbers (open symbols for 1/8, closed symbols for 1.0). Triangles, circles and squares denote data at $R_\lambda \approx 90$, 140, and 240, respectively. The dotted line shows the small r asymptote [Eq. (6)]. Dashed line at 1.608 is for comparison with experiments. The inset shows second-order structure function normalized by the scalar variance (which is not dependent on r), with dashed line at the value 2.0.

of normalized wavenumbers as observed in the higher-Reynolds-number grid experiments of Mydlarski and Warhaft[10] for temperature fluctuations in air with $Sc=0.7$. Experimental data from Fig. 12 of Ref. 10 are included for comparison in Fig. 2; the authors considered the apparent Obukhov–Corrsin constant in their data to be in broad agreement with the estimates by Sreenivasan.[9] A distinct bump is also seen in the one-dimensional longitudinal energy spectrum obtained from DNS.

As we shall see (Fig. 6, Sec. III B), this bump is a precursor to the -1 part of the spectral density that becomes more and more pronounced as Sc increases. Even a nascent presence of this feature at $Sc=1$ affects the $-5/3$ scaling range: Without the bump it is likely that one would see a more extensive stretch of the $-5/3$ scaling. This effect is particularly striking in the second-order structure function, which is the spatial equivalent of the one-dimensional spectrum. The classical result for spatial separations in the range $\eta \ll \eta_{\mathrm{OC}} \ll r \ll L$ is given by

$$D_{\phi\phi}(r) \equiv \langle(\Delta_r\phi)^2\rangle = C_2\langle\chi\rangle\langle\epsilon\rangle^{-1/3}r^{2/3}, \tag{5}$$

where, as shown in Ref. 1, $C_2=4.02C_\phi$. In our flow configuration we may distinguish between two-point differences in directions parallel and perpendicular to the mean gradient, as $\Delta_\parallel\phi(r)$ and $\Delta_\perp\phi(r)$. However, because isotropy at the intermediate scales is implied in Eq. (5), it is appropriate to make comparisons using DNS data averaged over r taken in three different coordinate directions.

Figure 3 shows the component-averaged structure function $\langle(\Delta_r\phi)^2\rangle$ normalized by the Obukhov–Corrsin variables as suggested in Eq. (5). It can be seen that, as the Reynolds number increases, results for $Sc=1$ show a tendency towards a flat scaling region (although, of course, a similar observation from data at yet higher Reynolds numbers not currently available would be even more convincing). The apparent scaling constant suggested by the data is higher than 1.61 (corresponding to $C_\phi \approx 0.4$ in Ref. 9) for $Sc=1$, but lower for $Sc=1/8$. In other words, in contrast to the behavior observed in the spectrum, the apparent scaling constant in structure functions shows a significant dependence on Schmidt number. We think that this is an artifact of the spectral bump which succeeds in masking the limited scaling region in the Fourier-transformed version. In support of this inference, we note that this apparent dependence on the Schmidt number weakens with increasing Reynolds number.

The limiting behaviors in Fig. 3 for small and large scale separation are both amenable to analysis, and can be used as checks on the quality of the data. In the limit of small r (i.e., $r \ll \eta_{\mathrm{OC}}$), Taylor series arguments imply that $\langle(\Delta_r\phi)^2\rangle$ grows like r^2, so that the normalized structure function shown in the figure behaves as

$$\frac{\langle(\Delta_r\phi)^2\rangle}{\langle\chi\rangle\langle\epsilon\rangle^{-1/3}r^{2/3}} = \frac{1}{6}\left(\frac{r}{\eta_{\mathrm{OC}}}\right)^{4/3}. \tag{6}$$

This is indicated by a dotted line. Its perfect agreement with the data (at small r) indicates that the small scales are adequately resolved. For large r, as values of ϕ at two points far apart in space become statistically independent, $\langle(\Delta_r\phi)^2\rangle$ is expected to approach a constant value equal to $2\langle\phi^2\rangle$. Asymptotic constancy of the structure function at larger r is illustrated in the inset, which shows that the ratio $\langle(\Delta_r\phi)^2\rangle/\langle\phi^2\rangle$ reaches a value close to 2. The correspond-

ing result for the normalized form in the main body of this figure is that it should decrease as $r^{-2/3}$. Indeed by using the time scale ratio $(K/\langle\epsilon\rangle)/\tau_\eta \approx (\frac{3}{2}\sqrt{15})R_\lambda$ we can show that the large-separation asymptote is

$$\frac{\langle(\Delta_r\phi)^2\rangle}{\langle\chi\rangle\langle\epsilon\rangle^{-1/3}r^{2/3}} \approx \frac{3R_\lambda Sc^{1/2}}{\sqrt{15}r_\phi}\left(\frac{r}{\eta_{OC}}\right)^{-2/3}, \tag{7}$$

where r_ϕ is the mechanical-to-scalar time scale ratio (see Table I, and end of Sec. II). Use of periodic boundary conditions on the computational domain implies that it is meaningful to compute structure functions only for r up to half of the length L_0 of each side of the domain. However, because of finite domain size (with L_0 only about six times of the integral length scale of the scalar field—which is 40% longer in the direction of the mean scalar gradient), the rate of approach to the large-r asymptote is somewhat distorted.

The mixed third-order structure function, defined as $D_{L\phi\phi}(r) \equiv \langle\Delta_r u(\Delta_r\phi)^2\rangle$ where $\Delta_r u$ is a longitudinal velocity increment in space, has a more fundamental role in similarity scaling. In particular, an exact result for intermediate r in the inertial-convective range was given by Yaglom,[20] as

$$\langle\Delta_r u(\Delta_r\phi)^2\rangle = -\tfrac{2}{3}\langle\chi\rangle r. \tag{8}$$

(Note that this relation was originally given by Yaglom with half the present scalar dissipation rate, and so the coefficient was 4/3 instead of the present 2/3.) In the limit of small r it is reasonable to use Taylor's series to write the approximation

$$\langle\Delta_r u(\Delta_r\phi)^2\rangle \approx S_{u\phi}\left\langle\left(\frac{\partial u}{\partial x}\right)^2\right\rangle^{1/2}\left\langle\left(\frac{\partial\phi}{\partial x}\right)^2\right\rangle r^3, \tag{9}$$

where $S_{u\phi}$ is the mixed gradient skewness defined by (see also Kerr[40])

$$S_{u\phi} \equiv \left\langle\left(\frac{\partial u}{\partial x}\right)\left(\frac{\partial\phi}{\partial x}\right)^2\right\rangle \Big/ \left\langle\left(\frac{\partial u}{\partial x}\right)^2\right\rangle^{1/2}\left\langle\left(\frac{\partial\phi}{\partial x}\right)^2\right\rangle. \tag{10}$$

Local isotropy relations for both the velocity and scalar fields further lead to

$$\langle\Delta_r u(\Delta_r\phi)^2\rangle \approx S_{u\phi}\left(\frac{\langle\epsilon\rangle}{15\upsilon}\right)^{1/2}\frac{\langle\chi\rangle}{6D}r^3 \tag{11}$$

and, finally, in normalized form[41]

$$\frac{\langle\Delta_r u(\Delta_r\phi)^2\rangle}{\langle\chi\rangle r} \approx \frac{S_{u\phi}}{6\sqrt{15}}\left(\frac{r}{\eta_B}\right)^2. \tag{12}$$

Figure 4 shows DNS results for the mixed structure function, in normalized forms suggested by Eqs. (8) and (12). As for the second-order structure function, we have taken an average over three coordinate components. With $S_{u\phi}$ taken to be of order -0.5 (see Table II), the behavior at small r indeed follows Eq. (12) for all Reynolds and Schmidt numbers in the data. Because of moderate Reynolds number in DNS, Eq. (8) is not attained exactly but nevertheless there is a sustained trend towards a plateau of height 2/3 (centered around $r/\eta_B \approx 30$ at $R_\lambda \approx 240$ and $Sc=1$). For larger values of r the curves also become more widely spaced as the range

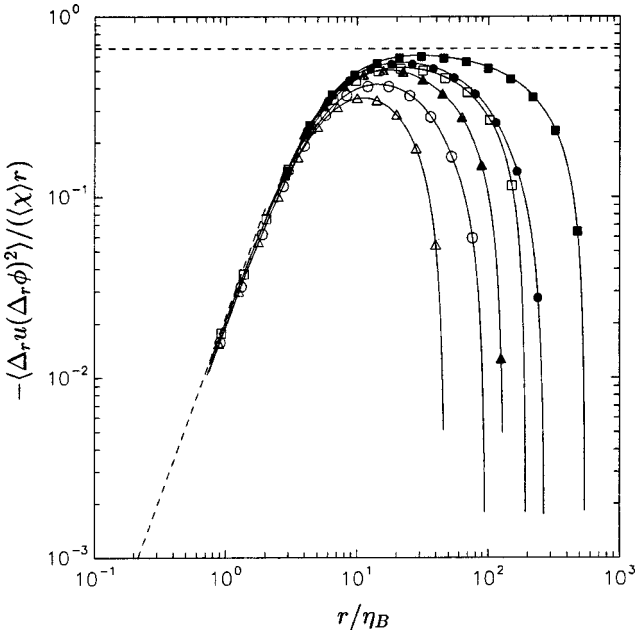

FIG. 4. Scaling of mixed third-order velocity-scalar structure function, compared with Yaglom's relation [Eq. (8)]. Symbols are same as in Fig. 3. Dashed line at 2/3 is for comparison with Yaglom's exact result.

of scales becomes wider with increasing R_λ and Sc. A rapid drop in the curves occurs in the limit of large r/η_B as $\langle\Delta_r u(\Delta_r\phi)^2\rangle$ itself approaches zero.

Some additional comments on the conditions of validity for Yaglom's relation [Eq. (8)] are appropriate. If the scalar field is stationary and isotropic, this relationship can be derived from the structure function equation

$$D_{L\phi\phi}(r) - 2D\frac{dD_{\phi\phi}(r)}{dr} = -\frac{2}{3}\langle\chi\rangle r, \tag{13}$$

provided that the diffusive term on the left-hand side (LHS) can be neglected in the inertial-convective range. Recently Orlandi and Antonia[42] studied the balance of terms in the structure function equation for decaying scalar fields. In agreement with their results, we find that the diffusive term is indeed small at intermediate scale ranges. Since the scalar fields studied by Orlandi and Antonia were decaying in time, they had to take account of nonstationarity in the balance of terms explicitly. However, in our simulations nonstationary contributions vanish when averaged over a sufficiently long period of time. One is then led to conclude that deviations from Eqs. (8) and (13) must be mainly caused by departures from local isotropy in the relevant scale range. Significant anisotropy is indeed seen in Fig. 5, which shows a comparison between normalized structure functions taken in different directions, for the case of $R_\lambda \approx 240$ with $Sc=1$. In particular, the structure function is systematically larger when r is taken parallel to the mean gradient direction. Since structure functions in experiments are usually measured in only one direction, this result suggests a need for caution in inferences on Yaglom's relation.

TABLE II. Mixed gradient skewness and flatness.

N	64	64	256	256	256	512	512	512	256	256	512	512
R_λ	38	38	38	38	38	38	38	38	140	140	240	240
Sc	1/4	1	4	8	16	16	32	64	1/8	1	1/8	1
$S_{u\phi}$	−0.66	−0.62	−0.61	−0.58	−0.55	−0.57	−0.54	−0.51	−0.57	−0.57	−0.60	−0.57
$S_{v\phi}$	−0.38	−0.42	−0.46	−0.47	−0.46	−0.46	−0.47	−0.46	−0.40	−0.44	−0.44	−0.45
$S_{w\phi}$	−0.31	−0.39	−0.46	−0.47	−0.46	−0.45	−0.45	−0.44	−0.41	−0.45	−0.45	−0.47
$F_{u\phi}$	2.25	2.06	1.96	1.91	1.85	1.90	1.85	1.78	2.03	1.98	2.25	2.16
$F_{v\phi}$	1.68	1.68	1.75	1.76	1.74	1.75	1.74	1.71	1.74	1.75	1.97	1.95
$F_{w\phi}$	1.60	1.63	1.71	1.71	1.68	1.68	1.68	1.65	1.79	1.79	1.99	1.96

B. Weakly diffusive scalars

For $Sc \gg 1$ Batchelor's result[7] for the scalar spectrum is

$$E_\phi(k) = q\langle\chi\rangle(\upsilon/\langle\epsilon\rangle)^{1/2}k^{-1}\exp(-q(k\eta_B)^2), \tag{14}$$

where the nondimensional coefficient q was presumed to be universal. Batchelor's theory was based on the assumption of persistent straining of the scalar field by small scale motions of characteristic time $\tau_\eta = (\upsilon/\langle\epsilon\rangle)^{1/2}$. Later Kraichnan[8] proposed a treatment that accounted for fluctuations of the strain rate and arrived at the form

$$E_\phi(k) = q\langle\chi\rangle(\upsilon/\langle\epsilon\rangle)^{1/2}k^{-1}(1+(6q)^{1/2}k\eta_B) \times \exp(-(6q)^{1/2}(k\eta_B)). \tag{15}$$

The main difference between the two expressions is in the viscous-diffusive range, $k\eta_B > 1$. In the viscous-convective range $1/\eta \ll k \ll 1/\eta_B$ both expressions give

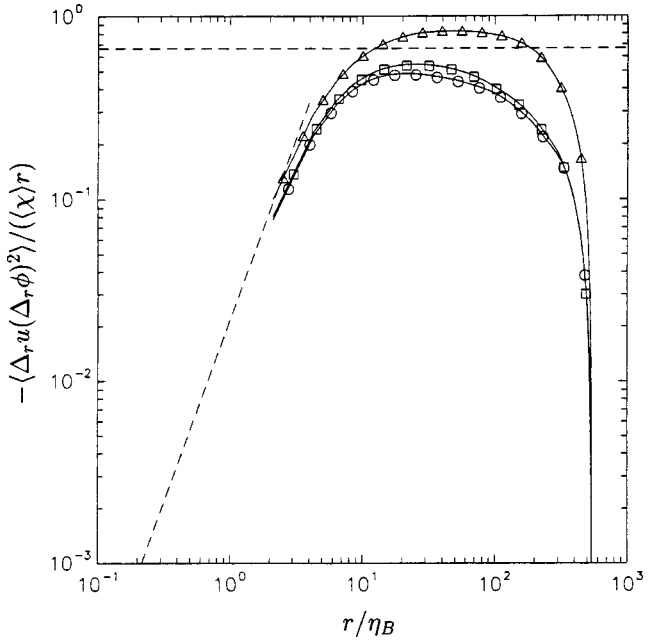

FIG. 5. Normalized third-order velocity-scalar structure function for $Sc = 1$ at $R_\lambda \approx 240$, with separation distance r taken in different coordinate directions (triangles, circles, squares for x, y, z, respectively).

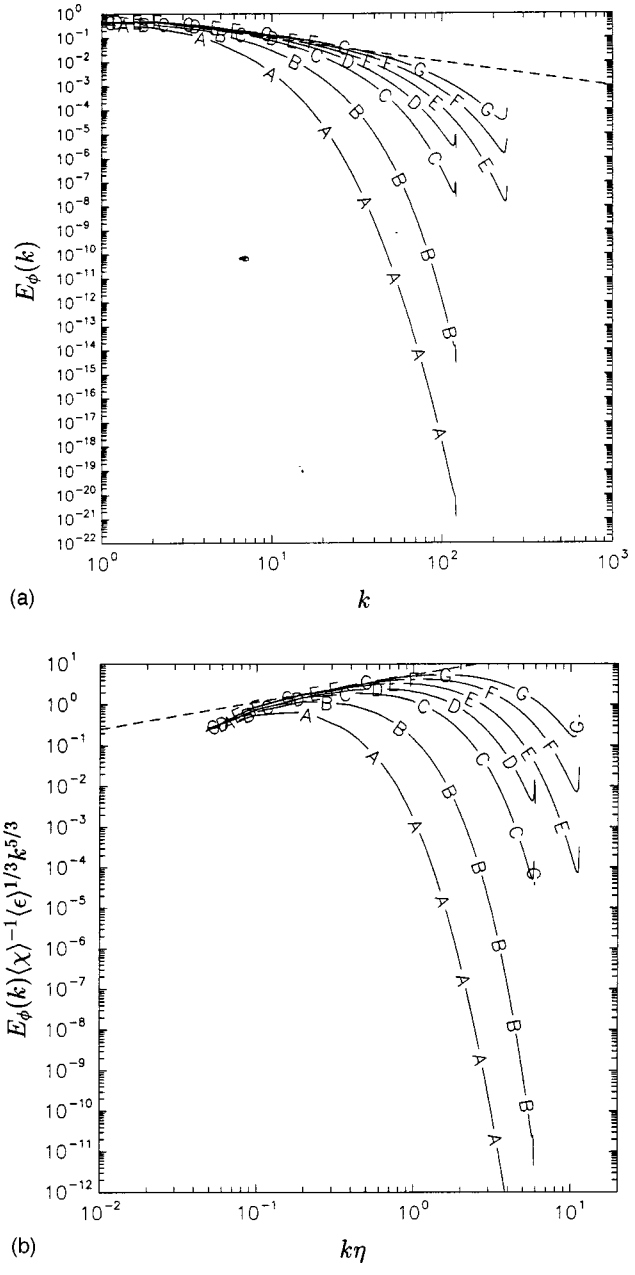

FIG. 6. (a) Three-dimensional spectra in un-normalized form at $R_\lambda \approx 38$ for scalars of Schmidt numbers 1/4, 1, 4, 8, 16, 32, 64 (lines A–G, respectively). The dashed line drawn has a slope of −1 on logarithmic scales. (b) Same data as in (a), but normalized in the same way as in Fig. 1. The dashed line drawn has a slope of 2/3 on logarithmic scales.

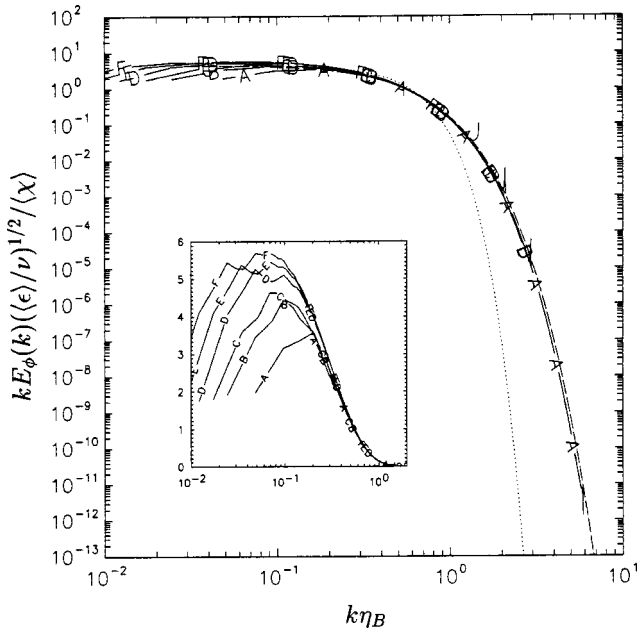

FIG. 7. Three-dimensional scalar spectrum at $R_\lambda \approx 38$ and $Sc = 1$, 4, 8, 16, 32, 64 (lines A–F, respectively) scaled by Batchelor variables. Classical k^{-1} scaling in the viscous-convective range would be illustrated by a plateau. Dotted curve for Batchelor's expression [Eq. (14)], dashed curve for Kraichnan's [Eq. (15)]. Inset shows the same data but in log-linear scales.

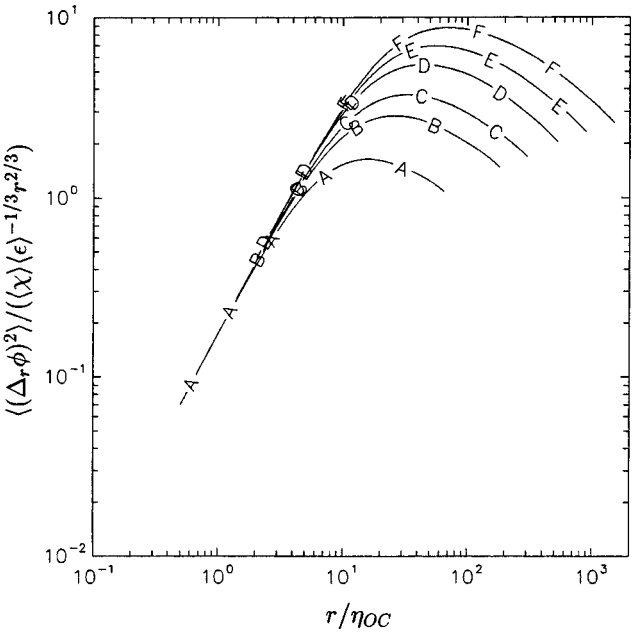

FIG. 9. Scaling of second-order structure function (similar to Fig. 3) for scalars of Schmidt numbers 1, 4, 8, 16, 32, 64 (lines A–F, respectively) at $R_\lambda \approx 38$.

$$E_\phi(k) = q\langle\chi\rangle(\upsilon/\langle\epsilon\rangle)^{1/2}k^{-1}, \tag{16}$$

which is commonly referred to as k^{-1} scaling. A substantial scale separation between η and η_B is required to observe this feature, but not necessarily a high Reynolds number. The value of q is generally estimated by either measurements or closure theories, but without universal agreement. For example, Batchelor[7] took $q=2$, whereas Qian[43] suggested $q = 2\sqrt{5}$, which was used for comparisons with DNS by Bogucki *et al.*[27]

Figures 6(a) and 6(b) show both un-normalized and normalized versions of the spectrum of different scalars at fixed $R_\lambda \approx 38$, with *Sc* varying between 1/4 and 64. The normalization used is the same as that in Fig. 1. Straight lines of appropriate slope are drawn to make comparisons with k^{-1} asymptotic scaling. It appears that the -1 region becomes increasingly well-defined with increasing *Sc*, and that the spectrum is progressively spreading out towards wavenum-

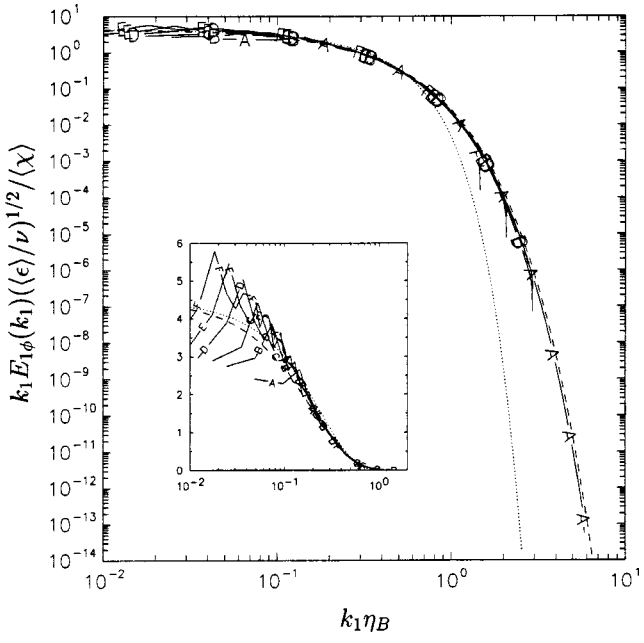

FIG. 8. One-dimensional spectrum version of Fig. 7.

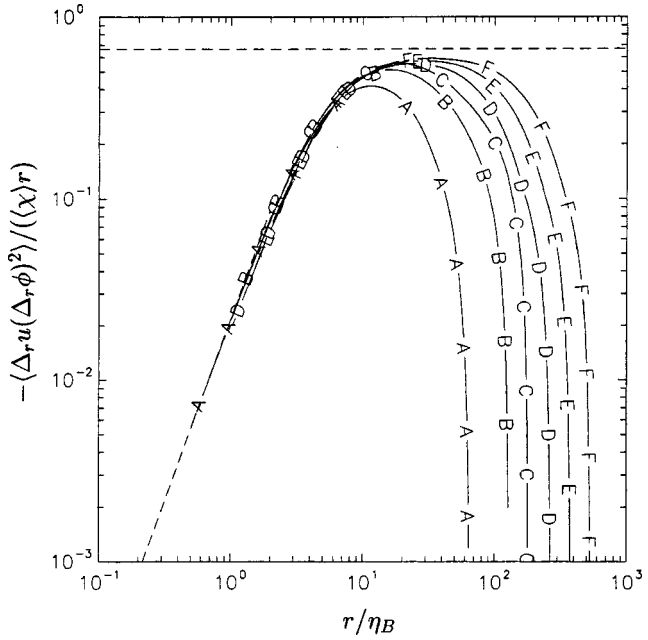

FIG. 10. Scaling of mixed third-order velocity-scalar structure function (similar to Fig. 4) for scalars of Schmidt numbers 1, 4, 8, 16, 32, 64 (lines A–F, respectively) at $R_\lambda \approx 38$.

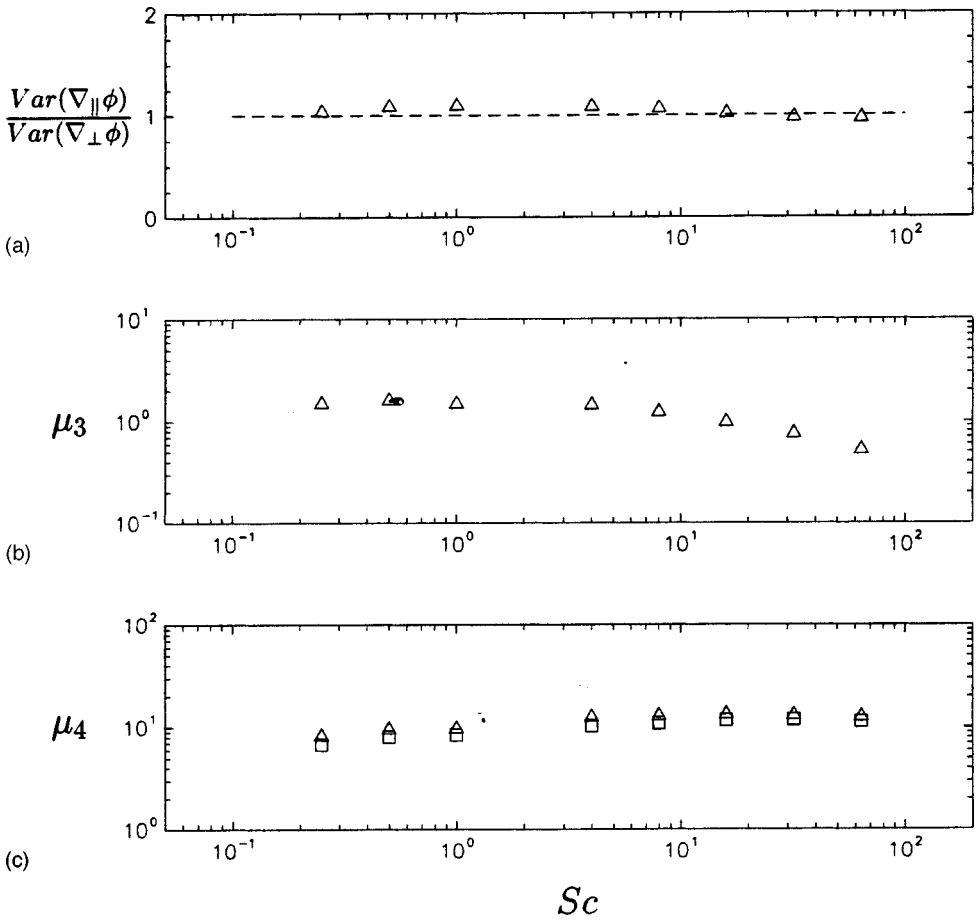

FIG. 11. Moments of scalar gradients in different coordinate components as a function of Schmidt number, at $R_\lambda \approx 38$. From top: (a) $\mathrm{Var}(\nabla_\parallel \phi)/\mathrm{Var}(\nabla_\perp \phi)$, (b) skewness of $\nabla_\parallel \phi$, (c) flatness of $\nabla_\parallel \phi$ (triangles) and $\nabla_\perp \phi$ (squares).

bers higher than $1/\eta$. As in Fig. 1, the spectra at low wavenumbers are nearly independent of Sc.

Figure 7 shows the spectrum normalized by Batchelor variables (as a function of $k\eta_B$) and compared with the expressions of Batchelor and Kraichnan. The data suggest the presence of k^{-1} scaling for $k\eta_B < 0.1$. Kraichnan's form is more accurate in the viscous-diffusive range, for which good agreement is found even for $Sc=1$. To infer the value of q needed for the best fit, we have also plotted the quantity $kE_\phi(k)(\langle \epsilon \rangle/\nu)^{1/2}/\langle \chi \rangle$ versus $k\eta_B$ (shown in the inset), such that q would be the height of a plateau at $k\eta_B \ll 1$. It appears that the value of q required for an optimum fit increases with Sc somewhat, being about 3.5 for $Sc=1$ but 5.5 for $Sc=64$.

As in the study of the Obukhov–Corrsin scaling (Sec. III A), to facilitate comparison with experiment we also plot the one-dimensional form of the spectrum scaled by Batchelor variables. This is shown in Fig. 8, with an inset using log-linear axes. One-dimensional versions of Batchelor's and Kraichnan's spectral forms are obtained by applying the spectral relationship

$$E_{1\phi}(k) = -\int_k^\infty \frac{E_\phi(k)}{k}\, dk \tag{17}$$

to Eqs. (14) and (15). The use of a linear axis for the normalized spectrum gives a more stringent test for k^{-1} scaling. Subject to some statistical deviation from isotropy in the lowest two wavenumber shells, the data support a k^{-1} scaling range, with a value of q that increases with Schmidt number (as already mentioned).

The effects of Schmidt number on the scaling of second-order structure functions for $Sc>1$ are shown in Fig. 9. For small r the Taylor-series result [Eq. (6)] in terms of Obukhov–Corrsin variables is seen to continue to hold, even for $Sc \gg 1$. Whereas an increase of Reynolds number has been seen (in Fig. 3) to promote the tendency for a plateau in the normalized structure function, an increase of Schmidt number apparently has no such effect. In the limit of larger r the data conform to Eq. (7) which is valid for all Schmidt numbers. Since the scaling used in Fig. 9 is chosen to produce a universal "collapse" at small scales, the "fanning-out" of curves with increasing Sc also reflects the existence of a wider range of scales in the scalar field at higher Sc.

Corresponding results for the mixed third-order structure function are shown in Fig. 10. It is interesting to note that, although Yaglom's relation [Eq. (8)] is traditionally associated with the inertial-convective range for $Sc \leqslant 1$ at high Reynolds number, the arguments leading to it are also increasingly valid at high Sc. Indeed it can be seen that our results at high Sc appear to approach the limit of Yaglom's relation for r in the intermediate range.

IV. LOCAL ISOTROPY: SCHMIDT NUMBER EFFECTS

Many indicators of varying degrees of sensitivity can be used as tests of local isotropy. For example, in Sec. III, we have discussed isotropy relations between spectra in one and three dimensions, and noted that structure functions show some differences depending on the direction of the spatial separation. Here, we focus mainly on statistics of scalar gradients in directions parallel ($\nabla_\parallel \phi$) and perpendicular ($\nabla_\perp \phi$) to the mean gradient, including their relationships with velocity gradient fluctuations.

Because of reflectional symmetry in the plane perpendicular to the mean gradient, all odd-order moments of $\nabla_\perp \phi$ are expected to be zero. Furthermore, local isotropy requires odd-order moments of $\nabla_\parallel \phi$ to vanish, and even-order moments of $\nabla_\parallel \phi$ and $\nabla_\perp \phi$ to be equal. Figure 11 presents second, third and fourth order moments of $\nabla_\parallel \phi$ and $\nabla_\perp \phi$, for Schmidt numbers 1/4 to 64 at $R_\lambda \approx 38$. The ratio of variances is close to unity, but this is not a sensitive indicator of local isotropy. More interesting is the behavior of the skewness of $\nabla_\parallel \phi$, which is nearly constant between $Sc = 1/4$ and about 4 but decreases steadily (perhaps as a power law) for higher *Sc*. A weaker trend of decrease at high Peclet number may also be present in results by Holzer and Siggia (Ref. 15; their Table III) based on two-dimensional synthetic velocity fields. The apparent trend of decreasing skewness at high Schmidt number is, however, just one facet of the deeper question of whether local isotropy would be recovered in the limit of infinite Schmidt number. In any case, the trend of decreasing skewness at high Schmidt number suggests that local isotropy becomes a better approximation. The positive skewness itself is usually[15,22,44] thought to be due to the occurrence of ramp-cliff structures of preferred orientation induced by the mean gradient. If so, a reduction of skewness may be the result of the orientation of these structures in space becoming more randomized. The effects of high Schmidt number on these structures have yet to be investigated in detail though a beginning has been made.[45]

We wish to emphasize that the observed values of the skewness of $\nabla_\parallel \phi$ do not decrease with increasing Reynolds number. On the other hand, the flatness factors show increasing closeness between $\nabla_\parallel \phi$ and $\nabla_\perp \phi$ at the highest Schmidt numbers. For a more complete picture we also study higher-order moments. Normalized third, fifth, and seventh moments (μ_3, μ_5, μ_7) of $\nabla_\parallel \phi$, shown in Fig. 12, seem to decrease with *Sc* for large *Sc*. (The situation for moments of yet higher orders is unclear because they are subject to large uncertainties in statistical sampling.) The rates of decrease depend on the order of the moment. It is clear that, if the seventh order moment is to ultimately reach the isotropic value of zero, the Schmidt number would have to be extremely high.

A positive skewness for $\nabla_\parallel \phi$ as seen in Figs. 11 and 12 (and Table II) means that large positive fluctuations are more likely than negative ones. The probability density function (PDF) of $\nabla_\parallel \phi$ in normalized form is shown in Fig. 13. The PDF becomes more nearly symmetric at higher *Sc*, which is consistent with the reduction in skewness noted above. Schmidt number effects appear to be primarily felt via increased probabilities for large negative fluctuations. The increasing ''width'' of the PDF at high Schmidt number also indicates increased non-Gaussianity and intermittency. The form of the PDF is apparently close to exponential in the range between 5 and 15 standard deviations. However, because of sampling limitations, the situation at the extreme tails is uncertain.

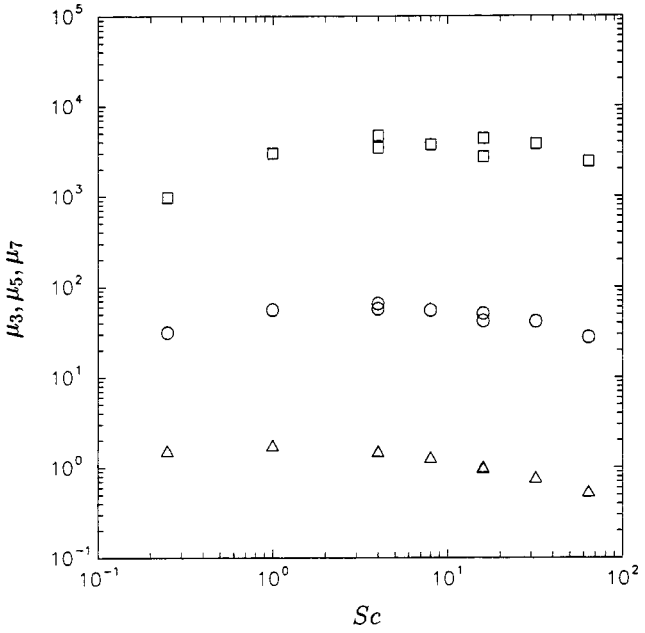

FIG. 12. Normalized third, fifth, and seventh-order moments (triangles, circles, squares, respectively) of $\nabla_\parallel \phi$ as a function of Schmidt number, at $R_\lambda \approx 38$.

Statistical relationships between fluctuations of velocity and scalar gradients, expressed as ''mixed'' derivative mo-

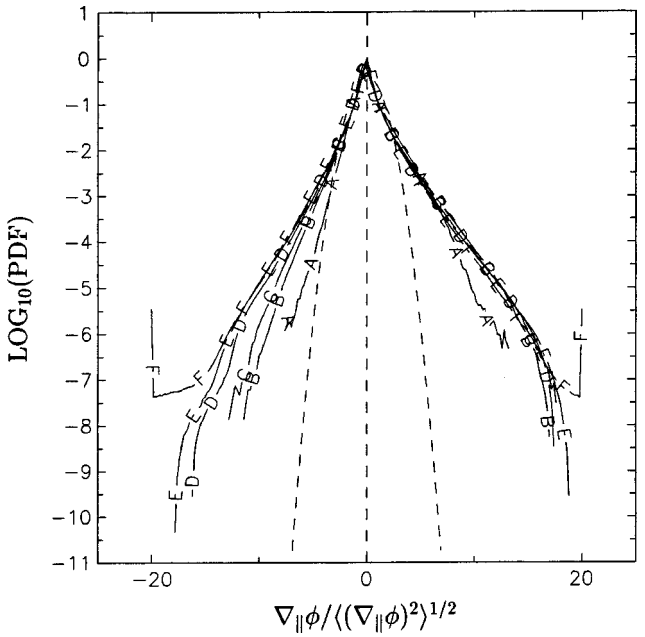

FIG. 13. Standardized PDF (shown as base-10 logarithm) of $\nabla_\parallel \phi$ for scalars of Schmidt numbers 1, 4, 8, 16, 32, 64 (lines A–F, respectively) at $R_\lambda \approx 38$. Dashed curve shows a Gaussian distribution for comparison.

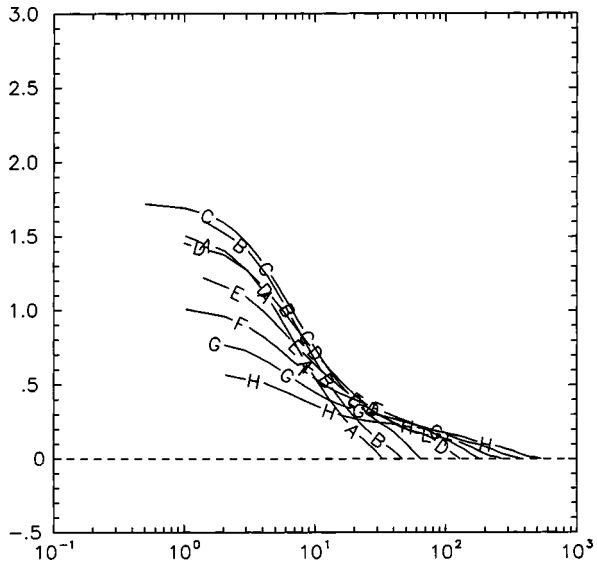

FIG. 14. The skewness structure function of $\Delta_\parallel \phi(r)$ [Eq. (19)] as a function of separation on Batchelor scales, for scalars of Schmidt numbers 1/4, 1/2, 1, 4, 8, 16, 32, 64 (lines A–H, respectively) at $R_\lambda \approx 38$. Dashed line shows Gaussian value of 0.

ments, are also relevant tests of isotropy. Similar to the mixed gradient skewness $S_{u\phi}$ [Eq. (10)], the mixed gradient flatness is defined by

$$F_{u\phi} \equiv \left\langle \left(\frac{\partial u}{\partial x}\right)^2 \left(\frac{\partial \phi}{\partial x}\right)^2 \right\rangle \Big/ \left\langle \left(\frac{\partial u}{\partial x}\right)^2 \right\rangle \left\langle \left(\frac{\partial \phi}{\partial x}\right)^2 \right\rangle. \tag{18}$$

Similar quantities $S_{v\phi}$, $S_{w\phi}$ and $F_{v\phi}$, $F_{w\phi}$ defined in the other (y and z) coordinate directions are also calculated. Numerical values listed in Table II show that the mixed skewness and flatness are generally larger in the direction of the mean scalar gradient. The contrast among different coordinate directions is strongest for low Schmidt number, but becomes less so at higher Reynolds number and/or Schmidt number. If gradients of velocity and scalar were statistically independent, the mixed skewness would be zero, and the mixed flatness would be unity. However, our data do not show a clear trend towards these asymptotic states.

In addition to single-point statistics presented above, it is useful to consider the degree of local isotropy as a function of scale size. In Fig. 14 we do this by showing the skewness structure function

$$\mu_3(r) \equiv \frac{\langle [\Delta_\parallel \phi(r)]^3 \rangle}{\langle [\Delta_\parallel \phi(r)]^2 \rangle^{3/2}}, \tag{19}$$

which is the skewness of the increment $\Delta_\parallel \phi(r)$. Similar to measurements in grid turbulence with transverse temperature gradient,[10] this function is found to be non-negative for all scale sizes r. Furthermore, contrary to local isotropy, this skewness becomes larger as r becomes smaller. For r of order η_B or less, different curves are seen to approach plateaus of different heights, corresponding to the skewness of $\nabla_\parallel \phi$ (see Table III). All curves approach zero for large r, because $\Delta_\parallel \phi(r)$ would then become a difference between two independent random variables. For high Sc (e.g., curve H for $Sc = 64$), there is a hint of an intermediate scaling range around 40 η_B, where the skewness becomes nearly independent of r. This observation suggests the emergence of an inertial-convective range where a small deviation from local isotropy exists at the level of the third-order moment.

V. INTERMITTENCY: EFFECTS FOR HIGH SCHMIDT NUMBERS

The small-scale intermittency of the passive scalar field is usually expressed in terms of the statistical properties and spatial structure of scalar gradients and the dissipation rate. Our prime concern here is how these characteristics depend on the Schmidt number, with observations of Reynolds number dependence also providing a useful contrast.

Table III also presents several moments of the scalar dissipation rate, and of its logarithm.[46] Because χ is a non-negative random variable, both its skewness and flatness factor are indicators of the occurrence of intense fluctuations that are large compared to the mean. In addition, the ratio $\sigma_\chi / \langle \chi \rangle$ (where σ_χ is the standard deviation) as well as the variance of $\ln \chi$ provide information on intermittency characteristics.[1,2] From Table III it is clear that, for a fixed Schmidt number, intermittency increases with Reynolds number.

TABLE III. Statistical moments of scalar gradients and the scalar dissipation.

N	64	64	256	256	256	512	512	512	256	256	512	512
R_λ	38	38	38	38	38	38	38	38	140	140	240	240
Sc	1/4	1	4	8	16	16	32	64	1/8	1	1/8	1
$\frac{\mathrm{Var}(\nabla_\parallel \phi)}{\mathrm{Var}(\nabla_\perp \phi)}$	1.05	1.11	1.10	1.08	1.07	1.00	0.99	0.98	1.04	1.05	1.08	1.05
$\mu_3(\nabla_\parallel \phi)$	1.54	1.53	1.49	1.27	0.98	1.01	0.78	0.54	1.72	1.46	2.14	1.63
$\mu_4(\nabla_\parallel \phi)$	8.47	9.97	12.9	13.3	12.6	13.7	13.5	13.0	11.6	14.7	18.6	21.2
$\mu_3(\nabla_\perp \phi)$	0.10	0.09	−0.05	−0.03	−0.02	−0.03	−0.02	−0.00	−0.09	−0.05	−0.01	0.02
$\mu_4(\nabla_\perp \phi)$	7.06	8.74	10.7	11.3	11.1	12.1	12.3	11.8	10.1	13.0	15.1	18.4
$\mu_3(\chi)$	5.53	5.88	7.04	7.22	6.82	8.13	8.08	7.47	6.66	7.63	10.0	10.5
$\mu_4(\chi)$	54.4	60.0	91.4	94.5	81.4	121	120	101	77.7	103	192	204
$\mathrm{Var}(\ln \chi)$	1.86	2.45	3.39	3.67	3.52	3.89	4.07	3.75	2.59	3.30	3.18	3.60
$\mu_3(\ln \chi)$	−0.15	−0.12	−0.17	−0.21	−0.18	−0.28	−0.30	−0.22	−0.06	−0.05	−0.00	0.03
$\mu_4(\ln \chi)$	3.22	2.97	2.84	2.86	2.84	2.90	2.91	2.82	2.89	2.81	2.87	2.85

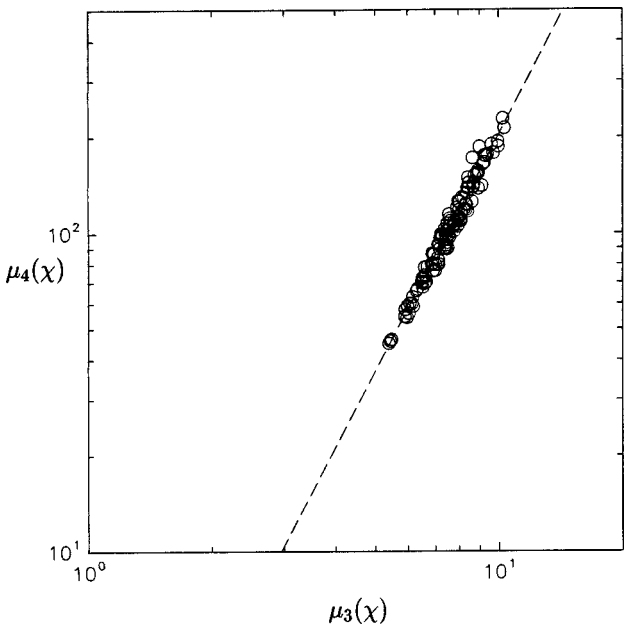

FIG. 15. Plot of flatness versus skewness for the scalar dissipation, at $R_\lambda \approx 38$ for $Sc=4$, 8, 16, 32, 64. Each data point represents one realization taken from 256^3 and 512^3 simulations. The dashed line is a least-square fit, of slope 2.47.

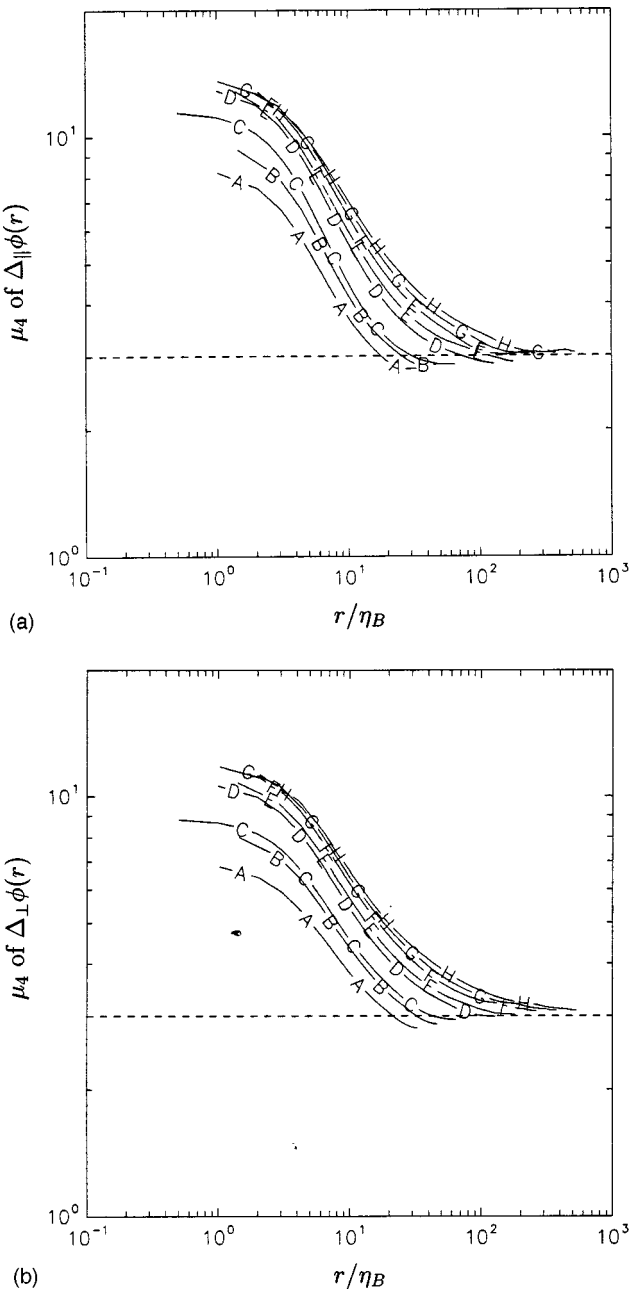

FIG. 16. (a) Flatness structure function of $\Delta_\parallel\phi(r)$ (in the direction of the mean scalar gradient), with symbols same as in Fig. 14. Dashed line shows Gaussian value of 3. (b) Same as (a), but for $\Delta_\perp\phi(r)$ (in the direction perpendicular to the mean scalar gradient).

To interpret Schmidt number effects we note first that, for $Sc=16$, all measures of intermittency are consistently stronger in the 512^3 simulations compared to 256^3, suggesting that intermittency may be underestimated if the grid resolution is not sufficiently refined. That is, it is not unlikely that the intermittency at $Sc=64$ (as well as at $Sc=1$ for $R_\lambda \approx 140$ and 240) is somewhat stronger than suggested in Table III. The flatness of the scalar dissipation, which is highly intermittent, is also subject to substantial statistical uncertainty. However, it is worth noting that, although the ensemble-averaged moments individually depend on *Sc*, a scatter plot of the flatness versus skewness (with one data point for each realization) is essentially universal independent of *Sc* (see Fig. 15). In other words, despite the substantial variability expected for higher-order moments, all realizations obey a systematic trend, which for $R_\lambda \approx 38$ in Fig. 15 is represented as a power-law variation with exponent approximately 2.4. (This exponent appears to be about the same at higher R_λ.)

Some general conclusions on the Schmidt number dependence can be drawn. It has been seen in Table III and Fig. 11(c) that the flatness factor of scalar gradients increases with *Sc* for low values of *Sc*, but varies little at higher *Sc*. Overall, it can be said that, consistent with other works in the literature,[24,47] all measures of intermittency for scalar dissipation at $Sc=1$ are more pronounced than for energy dissipation. In addition, it seems clear that the flatness of $\nabla_\parallel\phi$ stops increasing at $Sc\approx 4$, followed by $\nabla_\perp\phi$ beyond $Sc \approx 16$. This saturation of the flatness data suggests that some asymptotic state is reached as $Sc\to\infty$. Data on the skewness of $\ln\chi$ indicates that χ becomes closer to lognormal as *Sc* increases. Although departures from lognormality may still be present in higher-order moments of $\ln\chi$ (e.g., the normalized fifth-order moment is of the order -2.0), it appears that an approach to lognormality is plausible. (On the other hand, theories[48] based on rapidly varying Gaussian velocity fields suggest that χ has a stretched-exponential PDF in the limit of very high Schmidt number.)

Next, it is useful to consider intermittency as a function of scale size. Figures 16(a) and 16(b) show the flatness structure functions for the quantities $\Delta_\parallel\phi(r)$ and $\Delta_\perp\phi(r)$ with separation distance taken in the parallel and perpendicular directions, respectively. It can be seen that although the increasing trend ceases to hold for small scales when $Sc>4$, it does persist for intermediate scale sizes. This is especially true in the parallel direction. At lower Schmidt numbers

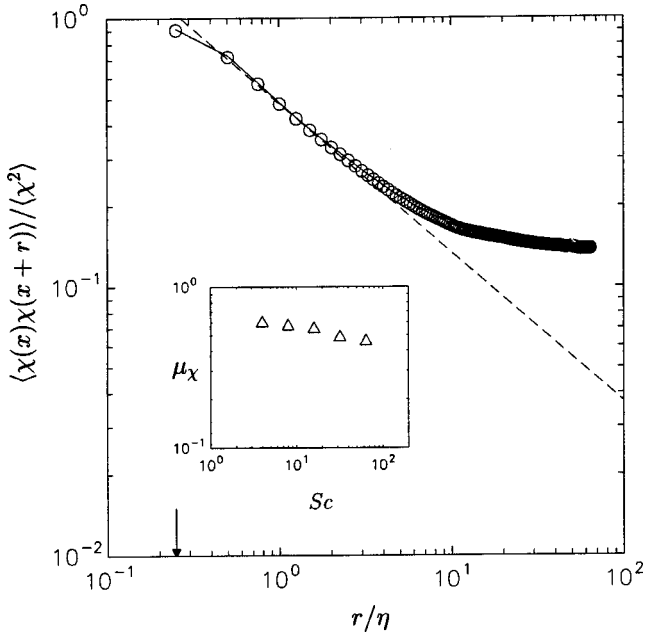

FIG. 17. Normalized two-point, second-order moment of scalar dissipation as a function of spatial separation [Eq. (20)] at $R_\lambda \approx 38$, $Sc=16$. The dashed line has a slope of -0.56. Inset shows the intermittency exponent μ_χ as a function of Schmidt number. The value of r that equals η_B is marked by an arrow on the r/η axis.

$\Delta_\parallel \phi(r)$ is more intermittent than $\Delta_\perp \phi(r)$, but this difference (which is an indication of anisotropy at scale size r) appears to vanish in the $Sc \gg 1$ limit.

A central feature of intermittency is the manner in which appropriate statistical properties depend on the averaging scale size. This effect is partly apparent in the previous figure but a more direct, and conventional, test is to measure the so-called intermittency exponent μ_χ in

$$\langle \chi(\mathbf{x})\chi(\mathbf{x}+\mathbf{r})\rangle \sim r^{-\mu_\chi}, \tag{20}$$

where, with local isotropy as at least a first approximation, dependence on the separation vector $\mathbf{r}$ is assumed to be through its magnitude r only. A brief summary of similar quantities for the energy dissipation rate was given by Sreenivasan and Kailasnath.[49] For scalars at high Schmidt number we are interested in this equation for scale size r varying nominally between η_B and η. In previous measurements[12] where the Batchelor scale was resolved in a low Reynolds number jet, μ_χ was found to be very close to zero. The Schmidt number for the dye used in the jet experiment was of the order 10^3. Here in the DNS data we can extract μ_χ at different Schmidt numbers and determine the Sc dependence. Figure 17 shows a log–log plot of $\langle \chi(\mathbf{x})\chi(\mathbf{x}+\mathbf{r})\rangle$ as a function of r and normalized by the mean-square of dissipation fluctuations, $\langle \chi^2\rangle$. To understand the general shape of the curve shown, we note that the two-point correlator $\langle \chi(\mathbf{x})\chi(\mathbf{x}+\mathbf{r})\rangle$ approaches its maximum value of $\langle \chi^2\rangle$ at small r, and its minimum value of $\langle \chi^2\rangle$ at large r. As expected, the scaling expressed in Eq. (20) is not readily apparent for small Sc, but if we insist on power laws, the estimated values of μ_χ as a function of Sc are as shown in the inset. The trend for this intermittency exponent (in the viscous-diffusive range) to decrease with Sc seems clear and its eventual decrease to zero as $Sc \to \infty$ seems plausible. Indeed most of the variation occurs for $Sc < 4$, which is consistent with the discussion above.

VI. CONCLUSIONS

We have studied the dynamics of turbulent scalar transport in direct numerical simulations by solving the advection-diffusion equation [Eq. (1)] in the presence of a uniform mean scalar gradient. The background turbulence is statistically stationary, homogeneous and isotropic. The Schmidt number varies between 1/4 and 64 for a fixed value of the Taylor microscale Reynolds number at $R_\lambda \approx 38$. The restriction to low R_λ is necessary to ensure adequate resolution of the scalar field. To provide further checks, some calculations are repeated for grid resolutions of 256^3 and 512^3. In addition, results for $Sc \leqslant 1$ are obtained from simulations at $R_\lambda \approx 140$ and 240. Together we have obtained a data base that allows us to learn about trends with respect to Sc—this being the main purpose of the paper. We have paid particular attention to Sc effects on the scalar spectra, structure functions, plus various quantities that characterize local isotropy and intermittency.

For moderate Sc, the spectra at the highest Reynolds numbers show a modest scaling in the inertial-convective region. The Obukhov–Corrsin constant is about 0.4 in one-dimensional spectra and 0.67 in three dimensions. The former is comparable to that in experiments.[9] The behaviors of scalar structure functions and mixed velocity-scalar structure functions are consistent with the existing theoretical framework provided that averages are taken over all three coordinate directions. There are conspicuous differences between statistics in directions parallel and perpendicular to the mean scalar gradient. There is no clear tendency for these differences to diminish with the Reynolds number, within the range considered here.

The Sc dependence in the weakly diffusive case ($Sc \gg 1$) is studied by using high grid resolution while holding the Reynolds number fixed. The spectra develop a -1 slope in the viscous-convective region consistent with Batchelor's theory. In the viscous-diffusive region, the spectral shape agrees better with the Kraichnan's form, which takes into account the intermittency of strain-rate fluctuations. However, there is one free parameter (q) in the spectral form. Best fits to the data show that this parameter depends weakly on Sc, but it is not clear if this dependence would persist at much higher Schmidt numbers. It is interesting that, even for $Sc \gg 1$, second-order structure functions obey the Obukhov–Corrsin scaling meant for Sc of the order unity. Furthermore, perhaps surprisingly, the form of Yaglom's equation for the mixed structure functions appears to be valid in the convective region even for $Sc \gg 1$.

An issue that has received considerable attention is the small-scale anisotropy of the scalar. A conclusion of the present work is that the usual measures of anisotropy diminish with increasing Sc. This suggests that a proper limit for local isotropy to work is $R_\lambda \to \infty$ and $Sc \gg 1$. A numerical value of $Sc = 4$ seems to be large enough to begin to see the

decline of anisotropy in several parameters. This is true also for most measures of intermittency based on scalar gradient and dissipation fluctuations. However, this particular value of *Sc* will most likely depend on the Reynolds number of the flow, and thus should not be assumed to be universal. The intermittency exponent for the scalar dissipation in the viscous-diffusive range appears to decrease (in magnitude) with *Sc*, and tends towards zero for very large *Sc* characteristic of dyes mixed by liquid turbulence.

It would be desirable to repeat these calculations for higher R_λ covering either the same range of *Sc* or larger. Although this range can be improved a bit by pushing the limit of modern computing power, it is unlikely that such an extension would be very substantial at this time. The increasing power of computers will make the problem worth revisiting in a few years' time. Useful information may also come from highly-resolved laboratory measurements.[50]

ACKNOWLEDGMENTS

We acknowledge valuable discussions with Andrzej Domaradzki, Rodney Fox, and Zellman Warhaft at various stages of this work, Laurent Mydlarski for providing experimental data from Ref. 10, and Haris Catrakis, Grisha Falkovich, Joerg Schumacher, and Prakash Vedula for comments on an earlier version of the paper. We gratefully acknowledge support from the National Science Foundation, via Grant Nos. CTS-0121030 (P.K.Y.) and CTS-0121007 (K.R.S.), as well as via NSF cooperative agreement ACI-9619020 through computing resources provided by the National Partnership for Advanced Computational Infrastructure at the San Diego Supercomputer Center.

[1] A. S. Monin and A. M. Yaglom, *Statistical Fluid Mechanics* (MIT, Cambridge, MA, 1975), Vol. II.
[2] U. Frisch, *Turbulence* (Cambridge University Press, Cambridge, U.K., 1995).
[3] K. R. Sreenivasan and R. A. Antonia, "The phenomenology of small-scale turbulence," Annu. Rev. Fluid Mech. **29**, 435 (1997).
[4] A. N. Kolmogorov, "The local structure of turbulence in an incompressible viscous fluid for very large Reynolds numbers," Dokl. Akad. Nauk SSSR **30**, 301 (1941).
[5] A. M. Obukhov, "The structure of the temperature field in a turbulent flow," Izv. Akad. Nauk. SSSR, Ser. Geophys. **13**, 58 (1949).
[6] S. Corrsin, "On the spectrum of isotropic temperature fluctuations in isotropic turbulence," J. Appl. Phys. **22**, 469 (1951).
[7] G. K. Batchelor, "Small-scale variation of convected quantities like temperature in turbulent fluid," J. Fluid Mech. **5**, 113 (1959).
[8] R. H. Kraichnan, "Small-scale structure of a scalar field convected by turbulence," Phys. Fluids **11**, 945 (1968).
[9] K. R. Sreenivasan, "The passive scalar spectrum and the Obukhov–Corrsin constant," Phys. Fluids **8**, 189 (1996).
[10] L. Mydlarski and Z. Warhaft, "Passive scalar statistics in high-Péclet-number grid turbulence," J. Fluid Mech. **358**, 135 (1998).
[11] C. H. Gibson and W. H. Schwarz, "The universal equilibrium spectra of turbulent velocity and scalar field," J. Fluid Mech. **16**, 365 (1963).
[12] R. R. Prasad and K. R. Sreenivasan, "Quantitative three-dimensional imaging and the structure of passive scalar fields in fully turbulent flows," J. Fluid Mech. **216**, 1 (1990).
[13] P. L. Miller and P. E. Dimotakis, "Measurements of scalar power spectra in high Schmidt number turbulent jets," J. Fluid Mech. **308**, 129 (1996).
[14] B. S. Williams, D. Marteau, and J. P. Gollub, "Mixing of a passive scalar in magnetically forced two-dimensional turbulence," Phys. Fluids **9**, 2061 (1997).
[15] M. Holzer and E. D. Siggia, "Turbulent mixing of a passive scalar," Phys. Fluids **6**, 1820 (1994).
[16] R. A. Antonia, E. Hopfinger, Y. Gagne, and S. Ciliberto, "Temperature structure functions in turbulent shear flows," Phys. Rev. A **30**, 2704 (1984).
[17] C. Meneveau, K. R. Sreenivasan, P. Kailasnath, and M. S. Fan, "Joint multifractal measures: theory and applications to turbulence," Phys. Rev. A **41**, 894 (1990).
[18] F. Moisy, H. Willaime, J. S. Andersen, and P. Tabeling, "Passive scalar intermittency in low temperature helium flows," Phys. Rev. Lett. **86**, 4827 (2001).
[19] L. Skrbek, J. J. Niemela, K. R. Sreenivasan, and R. J. Donnelly, "Temperature structure functions in the Bolgiano regime of thermal convection," Phys. Rev. E **66**, 036303 (2002).
[20] A. M. Yaglom, "On the local structure of a temperature field in a turbulent flow," Dokl. Akad. Nauk SSSR **69**, 743 (1949).
[21] K. R. Sreenivasan, "On local isotropy of passive scalars in turbulent shear flows," Proc. R. Soc. London **434**, 165 (1991).
[22] Z. Warhaft, "Passive scalars in turbulent flows," Annu. Rev. Fluid Mech. **425**, 161 (2000).
[23] M. R. Overholt and S. B. Pope, "Direct numerical simulation of a passive scalar with imposed mean gradient in isotropic turbulence," Phys. Fluids **8**, 3128 (1996).
[24] P. Vedula, P. K. Yeung, and R. O. Fox, "Dynamics of scalar dissipation in isotropic turbulence: a numerical and modeling study," J. Fluid Mech. **433**, 29 (2001).
[25] K. R. Sreenivasan and R. R. Prasad, "New results on the fractal and multifractal structure of the large Schmidt number passive scalars in fully turbulent flows," Physica D **38**, 322 (1989).
[26] G. Brethouwer, J. C. R. Hunt, and F. T. M. Nieuwstadt, "Microstructure and Lagrangian statistics of the scalar field with a mean gradient in isotropic turbulence," J. Fluid Mech. (in press).
[27] D. Bogucki, J. A. Domaradzki, and P. K. Yeung, "Direct numerical simulations of passive scalars with $Pr>1$ advected by turbulent flow," J. Fluid Mech. **343**, 111 (1997).
[28] P. K. Yeung, M. C. Sykes, and P. Vedula, "Direct numerical simulation of differential diffusion with Schmidt numbers up to 4.0," Phys. Fluids **12**, 1601 (2000).
[29] R. S. Rogallo, "Numerical experiments in homogeneous turbulence," NASA Tech. Memo. 81315 (1981).
[30] P. K. Yeung and Y. Zhou, "On the universality of the Kolmogorov constant in numerical simulations of turbulence," Phys. Rev. E **56**, 1746 (1997).
[31] K. R. Sreenivasan and P. K. Yeung, "The dissipation anomaly in passive scalars," preprint (2002).
[32] Z. Warhaft and J. L. Lumley, "An experimental study of the decay of temperature fluctuations in grid-generated turbulence," J. Fluid Mech. **88**, 659 (1978).
[33] V. Eswaran and S. B. Pope, "Direct numerical simulations of the turbulent mixing of a passive scalar," Phys. Fluids **31**, 506 (1988).
[34] S. B. Pope, *Turbulent Flows* (Cambridge University Press, Cambridge, U.K., 2000).
[35] P. K. Yeung and B. L. Sawford, "Random sweeping hypothesis for passive scalars in isotropic turbulence," J. Fluid Mech. **459**, 129 (2002).
[36] R. O. Fox, "The spectral relaxation model of the scalar dissipation rate in homogeneous turbulence," Phys. Fluids **7**, 1082 (1995).
[37] P. K. Yeung and S. B. Pope, "Differential diffusion of passive scalars in isotropic turbulence," Phys. Fluids A **5**, 2467 (1993).
[38] P. K. Yeung, "Multi-scalar triadic interactions in differential diffusion with and without mean scalar gradients," J. Fluid Mech. **321**, 235 (1996).
[39] J. R. Saylor and K. R. Sreenivasan, "Differential diffusion in low Reynolds number water jets," Phys. Fluids **10**, 1135 (1998).
[40] R. M. Kerr, "Higher-order derivative correlations and the alignment of small-scale structures in isotropic numerical turbulence," J. Fluid Mech. **153**, 31 (1985).
[41] Equation (11) differs from Eq. (21.91) of Ref. 1 except for unity Schmidt number. The subsequent appearance of the Batchelor scale in Eq. (12) without restriction on the Schmidt number (i.e., not merely for $Sc \gg 1$) is a consequence of the strain rate of the small scales appearing through the velocity gradient in $\langle \Delta_r u (\Delta_r \phi)^2 \rangle$ at small r. In the other limit of large r it is clear that isotropy in the velocity field implies that $\langle \Delta_r u (\Delta_r \phi)^2 \rangle$ approaches zero.
[42] P. Orlandi and R. A. Antonia, "Dependence of the nonstationary form of Yaglom's equation on the Schmidt number," J. Fluid Mech. **451**, 99 (2002).

[43]J. Qian, "Viscous range of turbulent scalar of large Prandtl number," Fluid Dyn. Res. **15**, 103 (1995).
[44]R. A. Antonia and C. W. Van Atta, "Structure function of temperature fluctuation in turbulent shear flows," J. Fluid Mech. **84**, 561 (1978).
[45]J. Schumacher and K. R. Sreenivasan, "Statistical and structural investigations in homogeneous shear flows," Bull. Am. Phys. Soc. **46**, 39 (2001).
[46]Some of the present numbers, especially those at R_λ 140 and 240, can be compared with those in Table III of Ref. 24. Some of the differences between the two sets of data are due to the fact that ensemble averages were not taken over the same numbers of realizations. By oversight, the numbers for $\sigma_\chi/\langle\chi\rangle$ given in Ref. 24 were for its square.
[47]L. P. Wang, S. Chen, and J. G. Brasseur, "Examination of hypotheses in the Kolmogorov refined turbulence theory through high-resolution simulations, Part 2. Passive scalar field," J. Fluid Mech. **400**, 163 (1999).
[48]M. Chertkov, G. Falkovich and I. Kolokolov, "Intermittent dissipation of a passive scalar in turbulence," Phys. Rev. Lett. **80**, 2121 (1998).
[49]K. R. Sreenivasan and P. Kailasnath, "An update on the intermittency exponent in turbulence," Phys. Fluids A **5**, 512 (1993).
[50]K. A. Buch and W. J. A. Dahm, "Experimental study of the fine-scale structure of conserved scalar mixing in turbulent shear flows: 1. $Sc \gg 1$," J. Fluid Mech. **317**, 21 (1996).